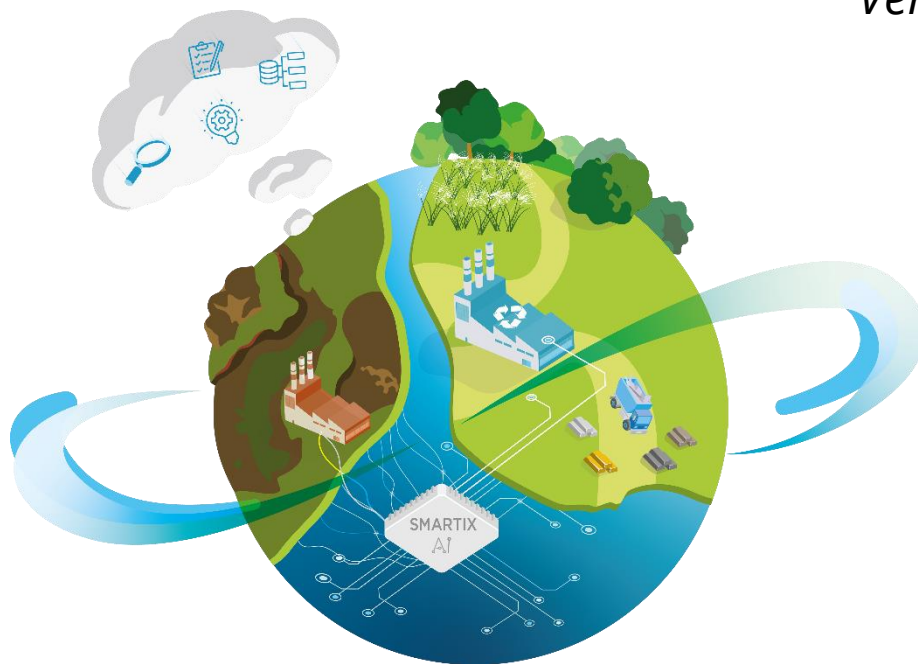


D. I3.2.3 Correlation report of characterization studies based on information from geophysical and traditional investigations

Itzel Isunza Manrique, David Caterina, Marc Dumont,
Frédéric Nguyen
ULiège
Version 1.0



1 CONTENTS

2	Introduction	2
2.1	Study area.....	2
2.2	Sampling survey design.....	3
3	Summary of the chemical analysis	3
3.1	Particle size distribution of chemical elements.....	5
3.2	Correlations between chemical elements	7
4	Correlations between chemical and geophysical data	7
4.1	From geophysical laboratory measurements	8
4.1.1	Electrical resistivity tomography (ERT) and induced polarization (IP) in time-domain 8	
4.1.2	Spectral induced polarization (SIP).....	10
4.2	From geophysical field measurements.....	14
5	Conclusions.....	16
6	References	17

2 INTRODUCTION

The following report presents the correlations we found between the geophysical measurements (carried out in laboratory and in the field) and geochemical analysis. First, we describe the sampling survey that was based on the geophysical results (targeted sampling). Then we present and discuss the chemical analyses conducted by CTP and study correlations between the chemical elements. We studied the correlations between the chemical analysis and the geophysical measurements of the methods that proved to be useful in the investigation of this site (see report DI3.2.1). These were the electrical resistivity tomography (ERT) and the induced polarization (IP) in time domain (using field and lab measurements) and the spectral induced polarization (SIP) for laboratory measurements.

2.1 STUDY AREA

The geophysical investigation of this site was focused on the zone of the white slags and the area of the old factory. Nevertheless, based on the geophysical measurements carried out in site and in the laboratory as well as the chemical analyses performed by CTP, in this report we focus on the area of the slag heap (see Figure 1).

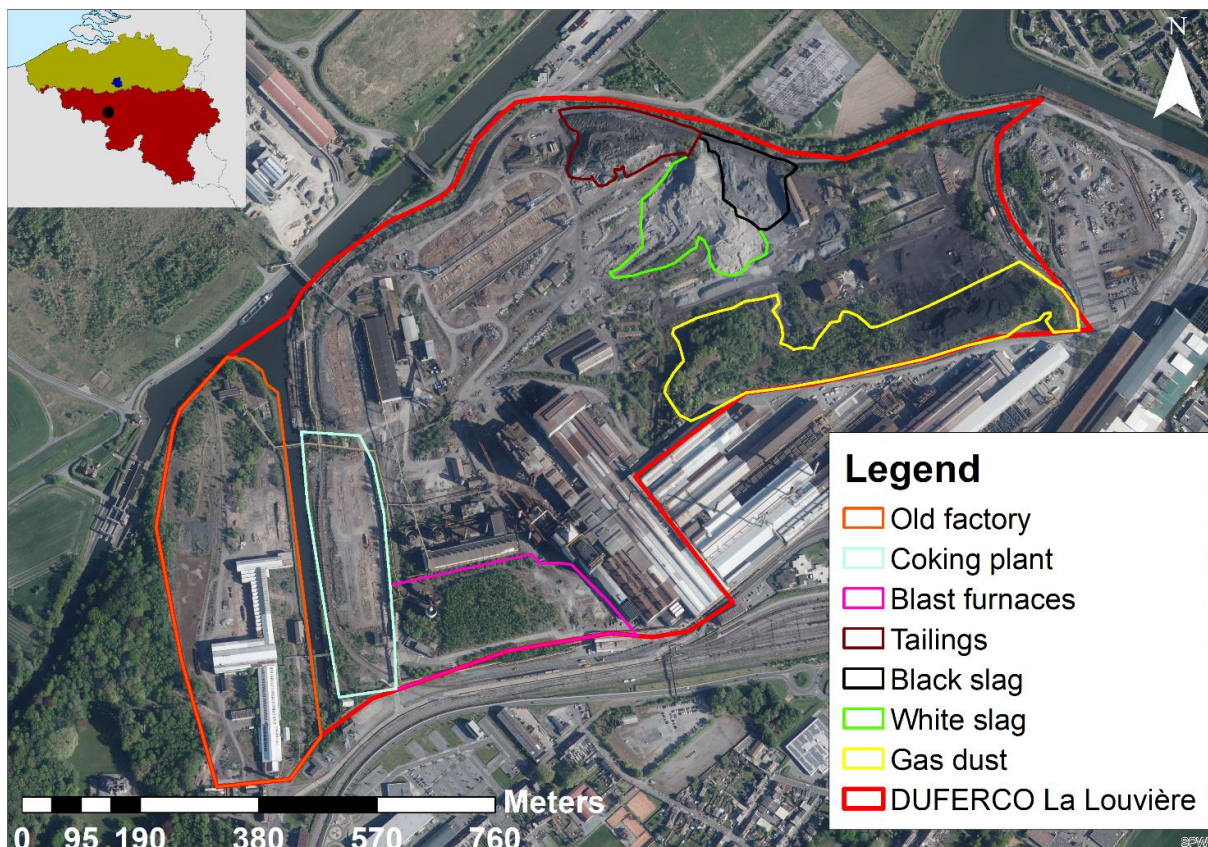


Figure 1: Aerial view of the Dufenco - La Louvière site with the delimitation of several potentially interesting areas for NWE-REGENERATIS.

2.2 SAMPLING SURVEY DESIGN

For the sampling survey of the slag heap we selected eight locations at which samples were collected at depths of 1, 3 and 5 m (see Figure 2). However, it was not possible to drill deeper where several vertical contrasts in the resistivity and chargeability models were observed. During the sampling survey 10- 15 kg of material was collected in buckets that were closed and stored in a cold environment. For more information on the survey as well as the chemical analysis, see report DI3.2.2.



Figure 2: Sampling plan for the slag heap.

3 SUMMARY OF THE CHEMICAL ANALYSIS

The geophysical lab measurements were carried out using columns of 1.5 dm³ with a mass between 1- 1.5 kg for each sample (see Figure 3). Then the same volumes were sent to CTP, who first sieved each sample and conducted a particle size distribution analysis and then XRF analysis per particle size. Therefore we have the elemental composition per particle size and in average for each sample. The chemical analyses were performed in terms of the elements presented in Table 1.



Figure 3: Column were the lab measurements of ERT, IP and SIP were carried out. The columns have a volume of 1.5 dm³, a diameter of 8 cm and height of 30 cm.

Table 1: Chemical elements studied in the XRF analyses

Element	Symbol
Fe	Iron
Si	Silicon
Ca	Calcium
Al	Aluminum
Mg	Magnesium
Mn	Manganese
Ni	Nickel
Cu	Copper
Sr	Strontium
K	Potassium
V	Vanadium
P	Phosphorus
S	Sulfur
Ti	Titanium
Cr	Chromium

3.1 PARTICLE SIZE DISTRIBUTION OF CHEMICAL ELEMENTS

The elements found in larger concentrations in most of the samples were Si, Ca, Fe, Mg, Al and Mn. For these elements the average content was at least larger than 1 % (wt). Figure 4 shows how these six elements are distributed along the different ranges of particle size. In this figure we can observe that each element has two plots: 1) the scatter plot shows the mass distribution vs size particle for all the samples and 2) the bar plot presents the average mass distribution for each size particle. The colorbar represents the concentration of each element for both plots. Note that the Si, Ca and Fe are found in the largest concentrations, followed by Mg, Al and Mn.

First, we can note that the mass in most of the samples is largely distributed in the smallest size particle ($< 63 \mu\text{m}$) and in the larger fractions ($> 5 \text{ mm}$). In terms of the elemental concentration, first, there are only a couple of samples that have large concentrations of Si, which is overall distributed in all the size particle ranges. For the calcium, note that most of the samples present an intermediate concentration distributed along all the size particle ranges although the average mass with larger concentrations of Ca is distributed in particle sizes $> 5 \text{ mm}$. In general, the Fe presents intermediate-to-large concentrations for particle sizes larger than 2.5 mm while the Fe content in the smallest particle size is very low ($< 63 \mu\text{m}$). Oppositely, the larger Mg content can be found in the smallest particle sizes. Then, in a similar distribution as the calcium, the larger concentrations of Al were also distributed along all the size particle ranges in general. Finally, although the Mn content is notably lower than the Fe content, the mass distribution of the Mn concentrations per size particle is very similar. The intermediate-to-large Mn content can also be observed at particle sizes larger than 2.5 mm.

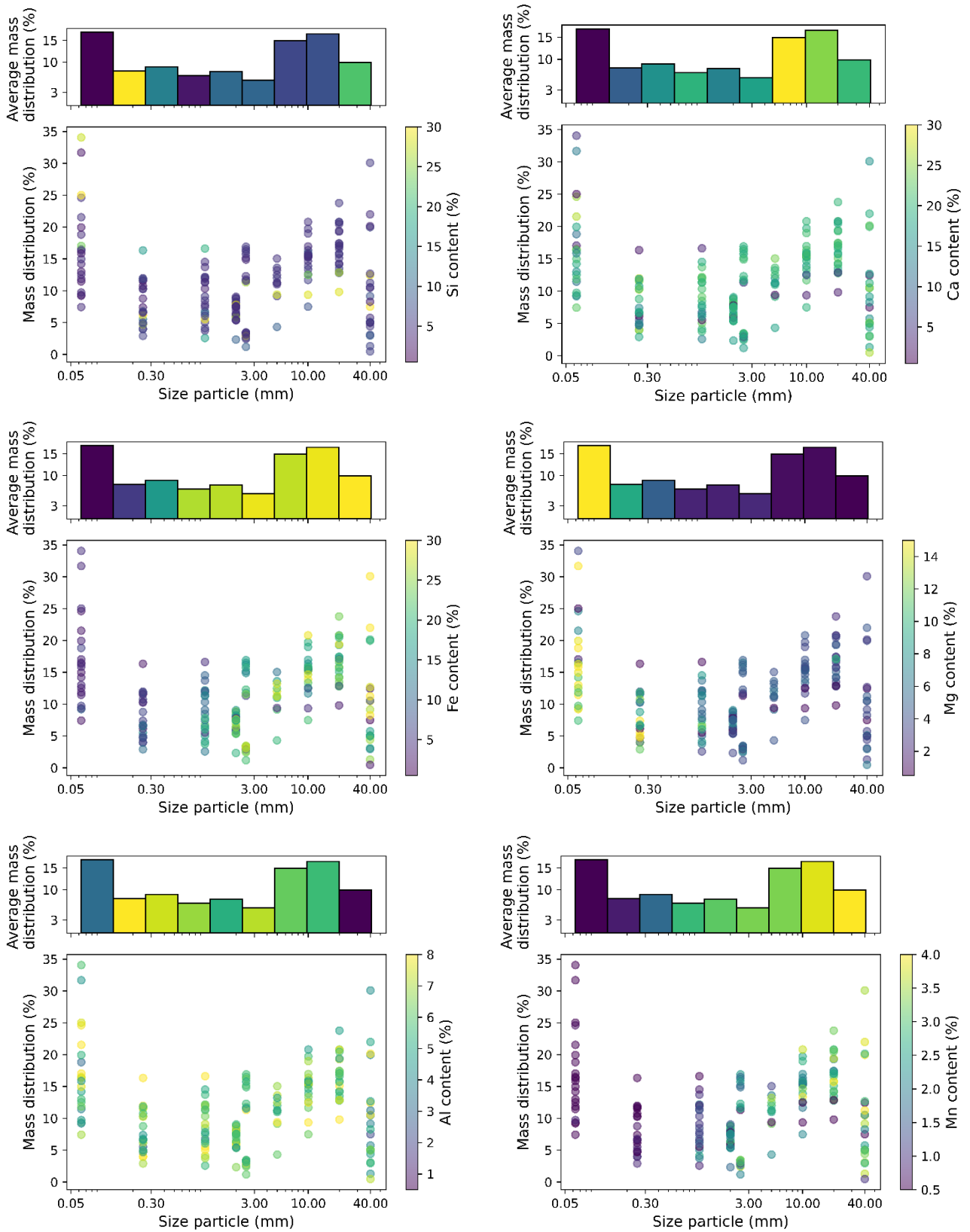


Figure 4: Particle size distribution of the chemical elements found in larger concentrations (> 1% wt.)

3.2 CORRELATIONS BETWEEN CHEMICAL ELEMENTS

In this subsection we studied the correlation between pairs of chemical elements (average content) found after the XRF analysis in all samples. As these variables have distinct ranges of average content (wt. %), e.g., maximum values of Fe content are around 30 % while Cu content is smaller than 1%, we first applied a standardization to compare all the elements. The standardization consists of removing the mean and scaling the data so that the variance is equal to one, i.e., subtract the mean of the data and divide by standard deviation. Then we computed the pairwise correlations coefficient of the standardized variables using Person's method (see correlation matrix in Figure 5). Note that in the correlation matrix the strong and positive relations are presented in blue while the strong and negative relations are shown in beige. Therefore, strong positive correlations between Mn-V, K-Si, Ti-Si, Cr-Mg, Ti-K and Cr-K and strong negative correlations between Ca-Si, and Al-Fe.

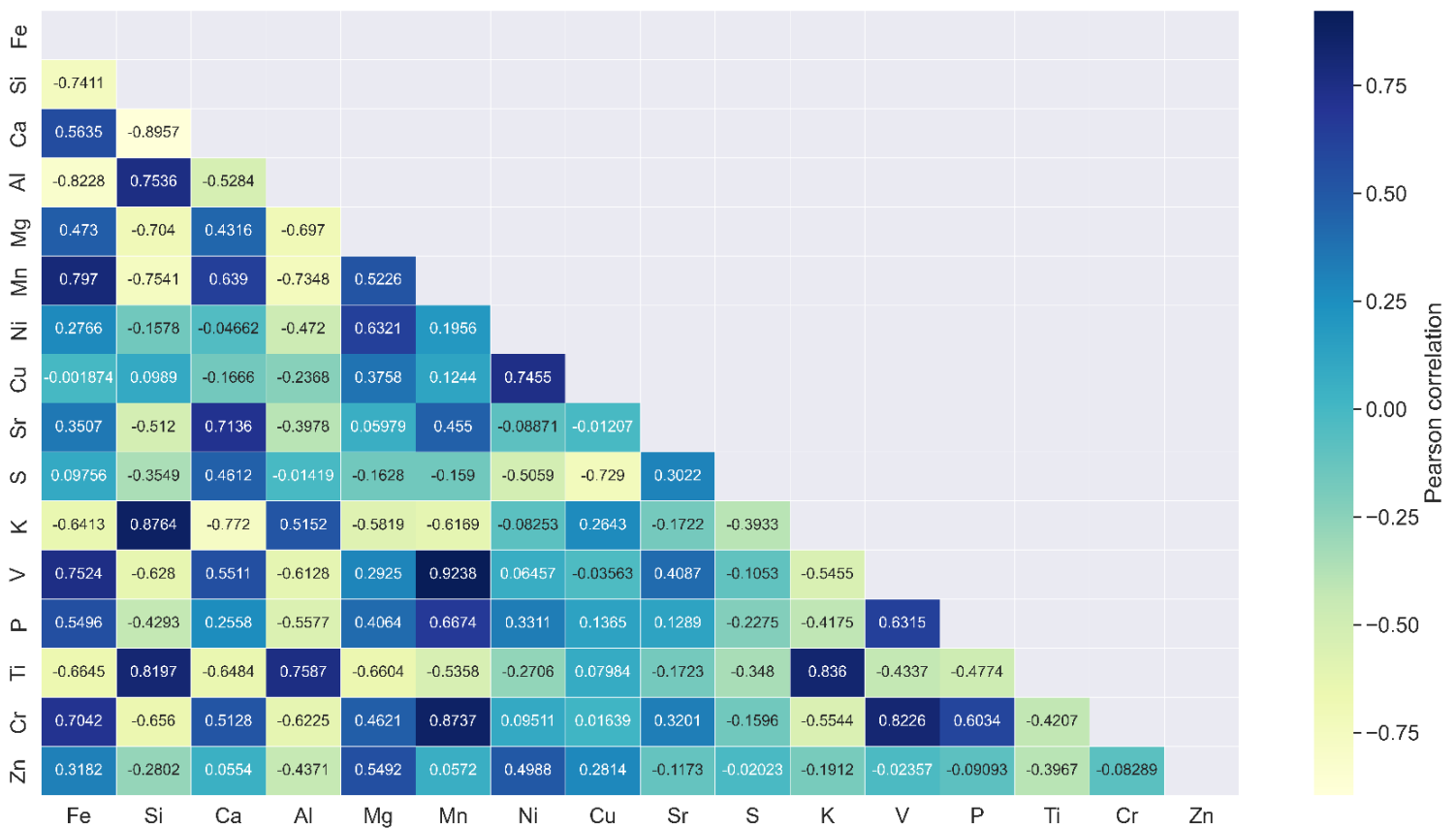


Figure 5: Pearson's correlation coefficient matrix of the average content elements measured in all samples

4 CORRELATIONS BETWEEN CHEMICAL AND GEOPHYSICAL DATA

The geophysical survey conducted in the slag heap mapped the entire volume using a 3D ERT and IP acquisition. Then, the samples that were collected in the field were used to measure ERT, IP and SIP in the lab and subsequently the XRF analysis were conducted in the same material.

Therefore, in this section we first present the correlations found between the elemental composition of the samples and the geophysical data measured in the laboratory and secondly, the correlations between the chemical data and the geophysical data measured in the field.

4.1 FROM GEOPHYSICAL LABORATORY MEASUREMENTS

4.1.1 Electrical resistivity tomography (ERT) and induced polarization (IP) in time-domain

The ERT and IP measurements were performed using 4 electrodes similar to a Wenner array (see Fig. 3) using the system Terrameter LS- ABEM. Electrical (direct) current was injected for 2 s and voltage decay was measured for 1.86 s after switching the current off.

Similarly to the previous section, we computed the Pearson's correlation coefficient matrix of the average content of some elements as well as the electrical resistivity (ρ) and chargeability (C) measured in the laboratory. As the data have different units, all variables were previously standardized in order to be compared pairwise. We only include the elements that presented correlation coefficients larger than 0.3 with the geophysical variables. The correlation coefficient matrix is shown in Figure 6.



Figure 6: Pearson's correlation coefficient matrix of the average content of some elements and the geophysical data measured in all samples

In the matrix we can observe strong positive correlations between the resistivity and the average content of K, Si and Ti, which means that the resistivity increases with the concentration of these elements. However, close inspection shows that the linear correlations observed with

the resistivity are rather biased by the presence of two clear clusters of different resistivity ranges (see Figure 7) and this indicates that there are at least two types of materials in the analyzed samples.

Then, for the linear correlations in terms of the chargeability we observe the strongest positive coefficients with the V, Mn, Cr and Fe. These linear relationships are displayed in Fig 8 where we can observe a smoother increase of chargeability values as compared with the resistivity.

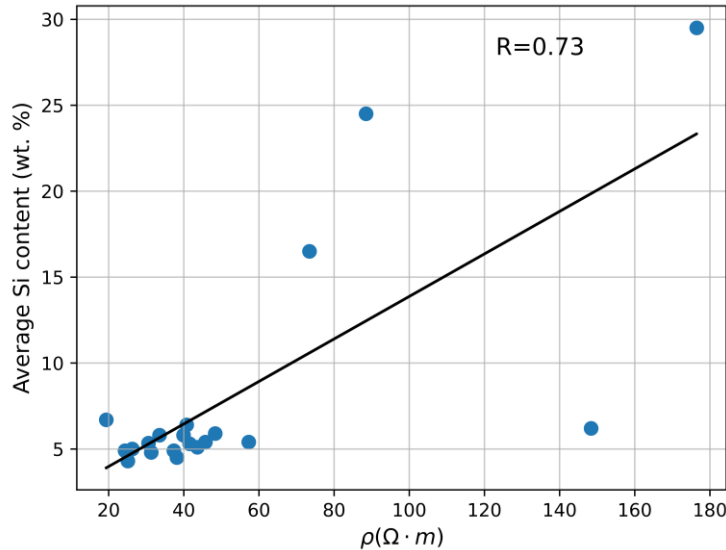


Figure 7: Linear relationship between average Si content and the resistivity. Correlation coefficient is also indicated.

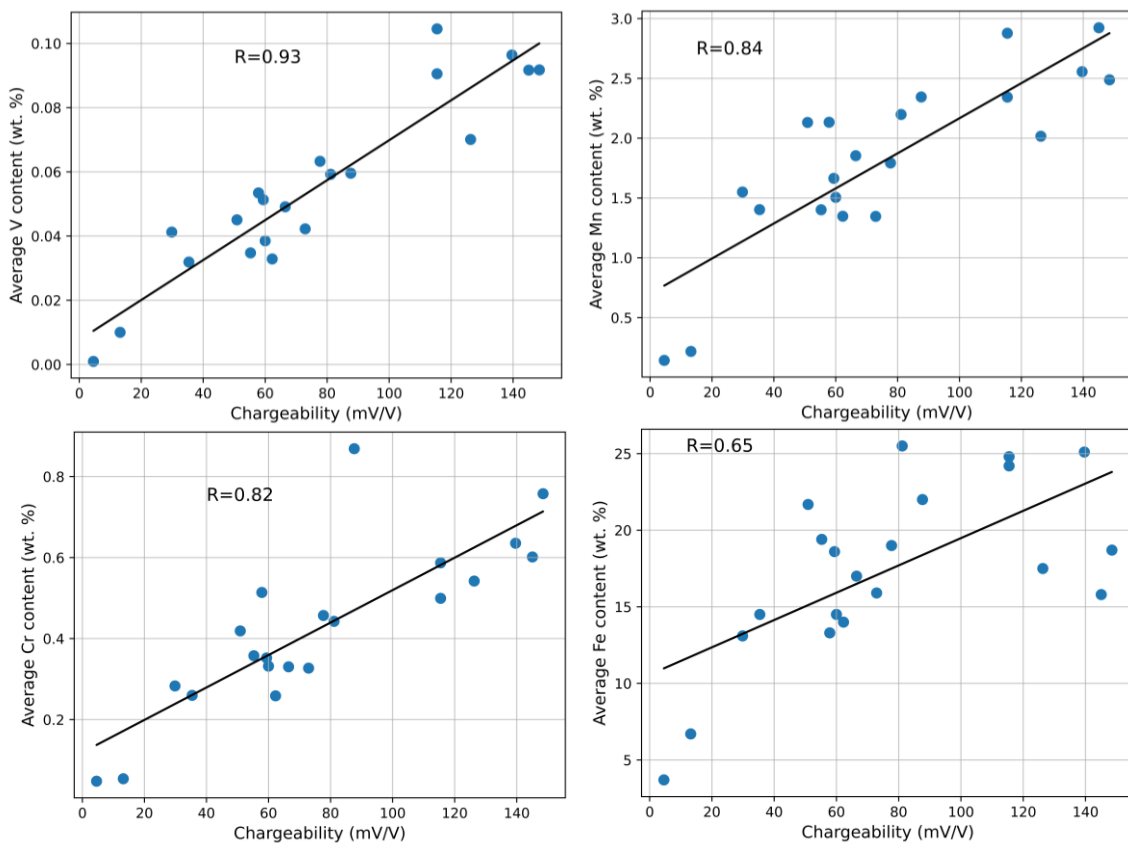


Figure 8: Linear relationship between chargeability and average content of V, Mn, Cr and Fe. The correlation coefficients are expressed in each plot.

Note that the strongest linear correlation was computed for the relationship between the chargeability and the average V content followed by the correlations of C- Mn and C- Cr, despite the low concentrations of these elements. Additionally in the correlation matrix we can observe a strong positive correlation between the same elements and the average Fe content although the correlation coefficient of C- Cr is slightly smaller. Therefore, the concentration of V increases with the concentration of Mn, Cr and Fe, which leads to an increase of chargeability (that may be a suitable parameter to discriminate the concentration of these elements).

In addition to the (at least) two clusters than can be distinguished in Figure 7 for the relation ρ -Si, we can identify three clusters in the plot of the average V content and chargeability. To integrate this information we used a cross-plot of chargeability vs resistivity with a colorbar representing the average V content (see Figure 9), where we can identify three clusters of low (blue circle), intermediate (orange circle) and large values (red circle) of average V content. This plot shows the ability that both resistivity and chargeability have to potentially differentiate materials of different composition.

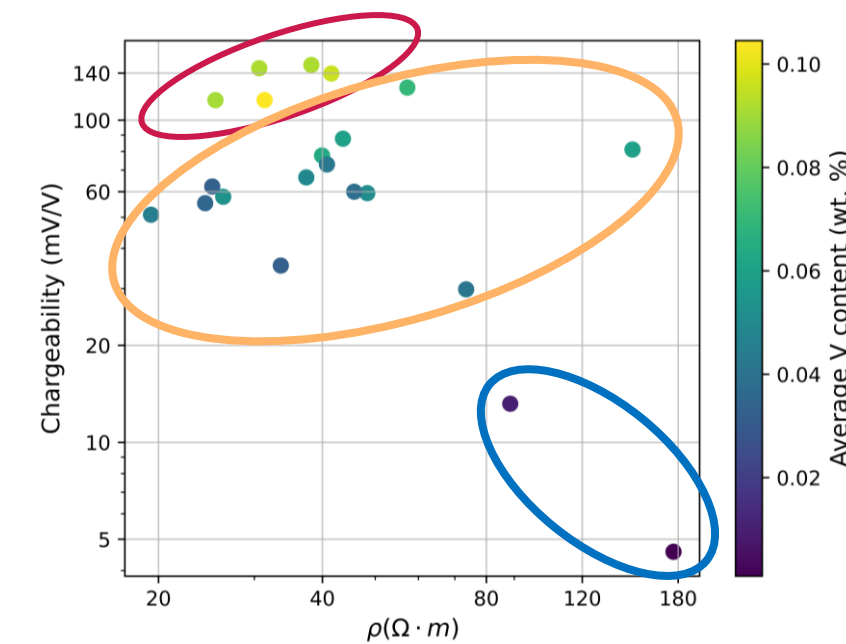


Figure 9: Cross-plot of chargeability vs resistivity. The colorbar represents the average V content (wt. %) and the circles of colors represent the different clusters

4.1.2 Spectral induced polarization (SIP)

SIP is also known as complex resistivity method and it can be seen as an extension of ERT, yet the SIP measurements are performed in frequency-domain and using an alternating current injection. SIP conducted both in the laboratory and in the field, represents a promising method to investigate the chemical form and physical properties of metallurgical residues as well as dynamic processes affecting them (Florsch et al. 2011; Martin et al. 2021; Placencia-Gómez et

al. 2015; Qi et al. 2018). Integrated approaches to study these type of wastes may include and/or integrate measurements in the field, targeted sampling, laboratory measurements and chemical or mineralogical analysis.

We carried out the SIP measurements using the same samples' volumes (and same columns) than the ERT/IP measurements. We used the system ZEA-2-SIP04-V05 Forschungszentrum Jülich (Zimmermann et al. 2010). Overall, in the SIP results we observe that the spectra of conductivities (or real component σ') increases with frequency, the imaginary component of the conductivity (σ'') have spectra of several shapes and finally for most of the samples the phase spectra (Φ) present a characteristic peak centered at a frequency around 1 Hz. Figure 10 shows the SIP spectra of some samples and the legend indicates the sample identifier, such as S1_5 refers to sample S5 collected at a depth of 5 m. Location of the samples are shown in Figure 2.

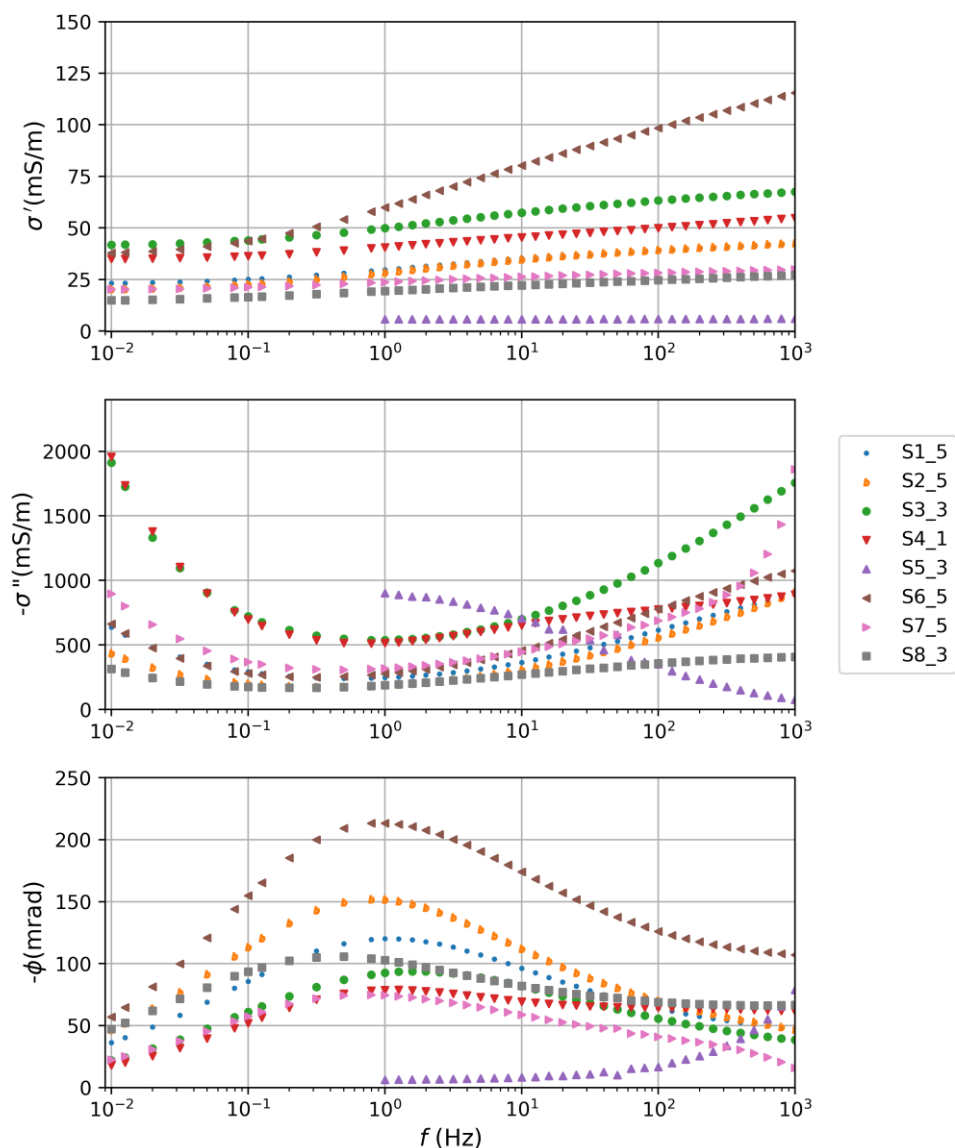


Figure 10: Overview of SIP spectra measured in the laboratory.

First, we studied the correlations between the measured spectra and the chemical analysis of XRF. For example, Figure 11 shows the SIP spectra of all samples with a colorbar representing

the average Fe content. In this figure we can note overall that some spectra with the largest magnitude of σ' present also the largest Fe content. The σ'' spectra corresponding to samples of intermediate to large Fe content present the same shape, spectra decrease at a frequency of around 1 Hz. Finally in the phase spectra we can note that, overall, the maximum magnitude (value of the peak phase observed at relaxation frequency) increase with the average Fe content.

Afterwards we studied the linear correlations between the concentration of different elements and the magnitude of the SIP spectra $\{\sigma', \sigma'', \Phi\}$ at the relaxation frequency or where the peak is observed. As an example, Figure 12 illustrates the linear correlation between the maximum phase magnitude ($|\Phi|_{\max}$) and the average Fe content. Finally, Figure 13 displays the correlation coefficient matrix including the average content of all the elements and the magnitude of σ', σ'', Φ at the maximum phase peak.

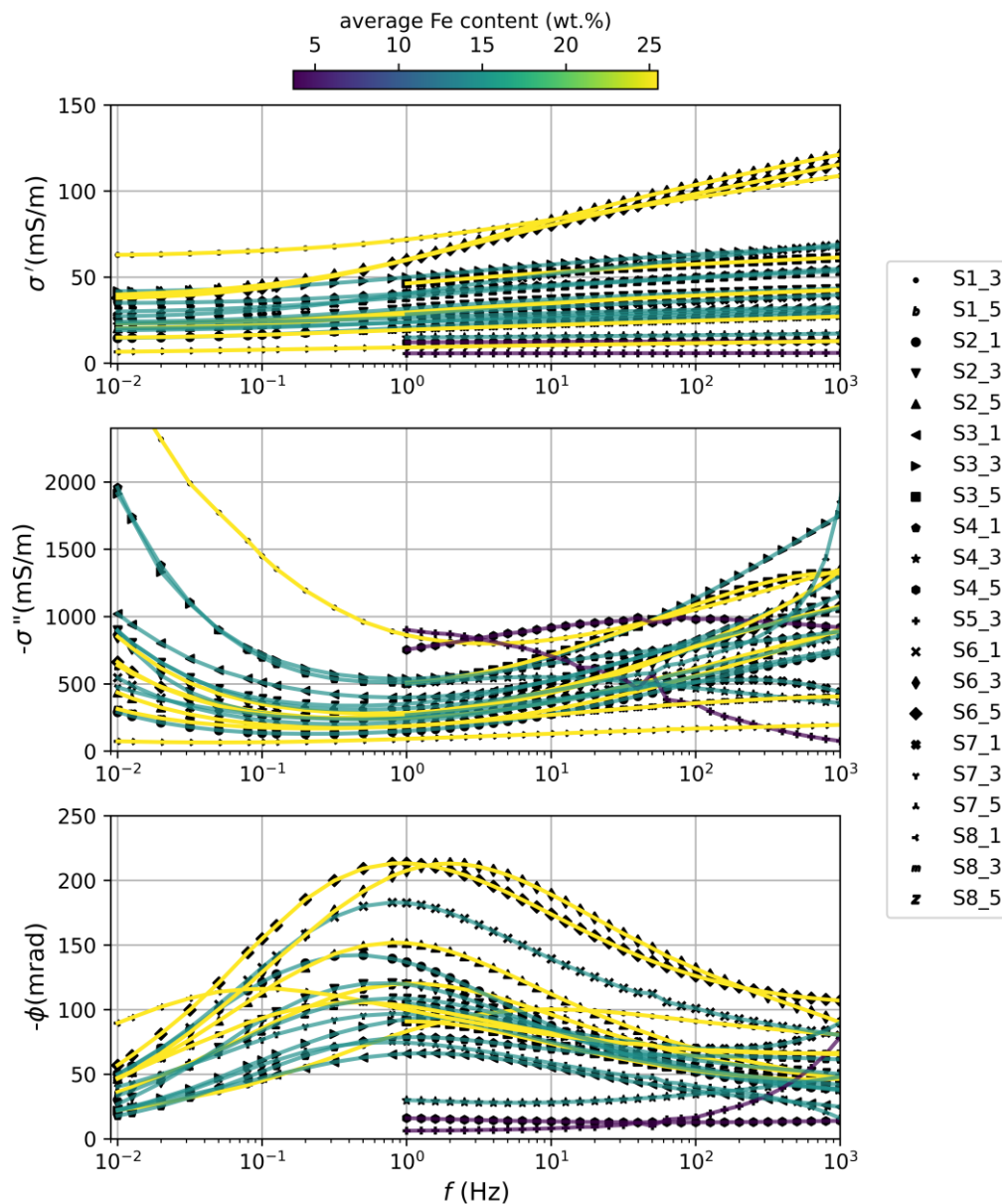


Figure 11: SIP spectra of all samples together with the average Fe content.

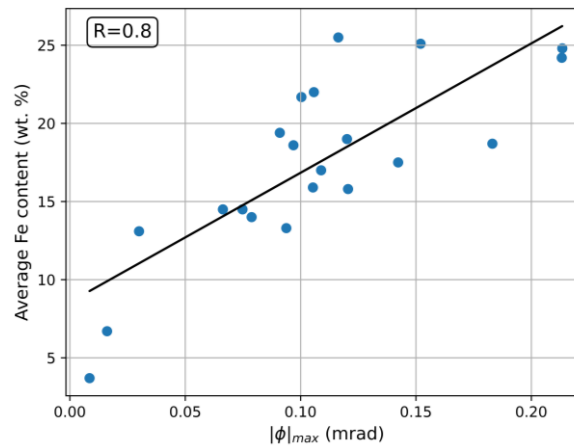


Figure 12: Linear relationship and correlation coefficient between average Fe content and the maximum phase magnitude.

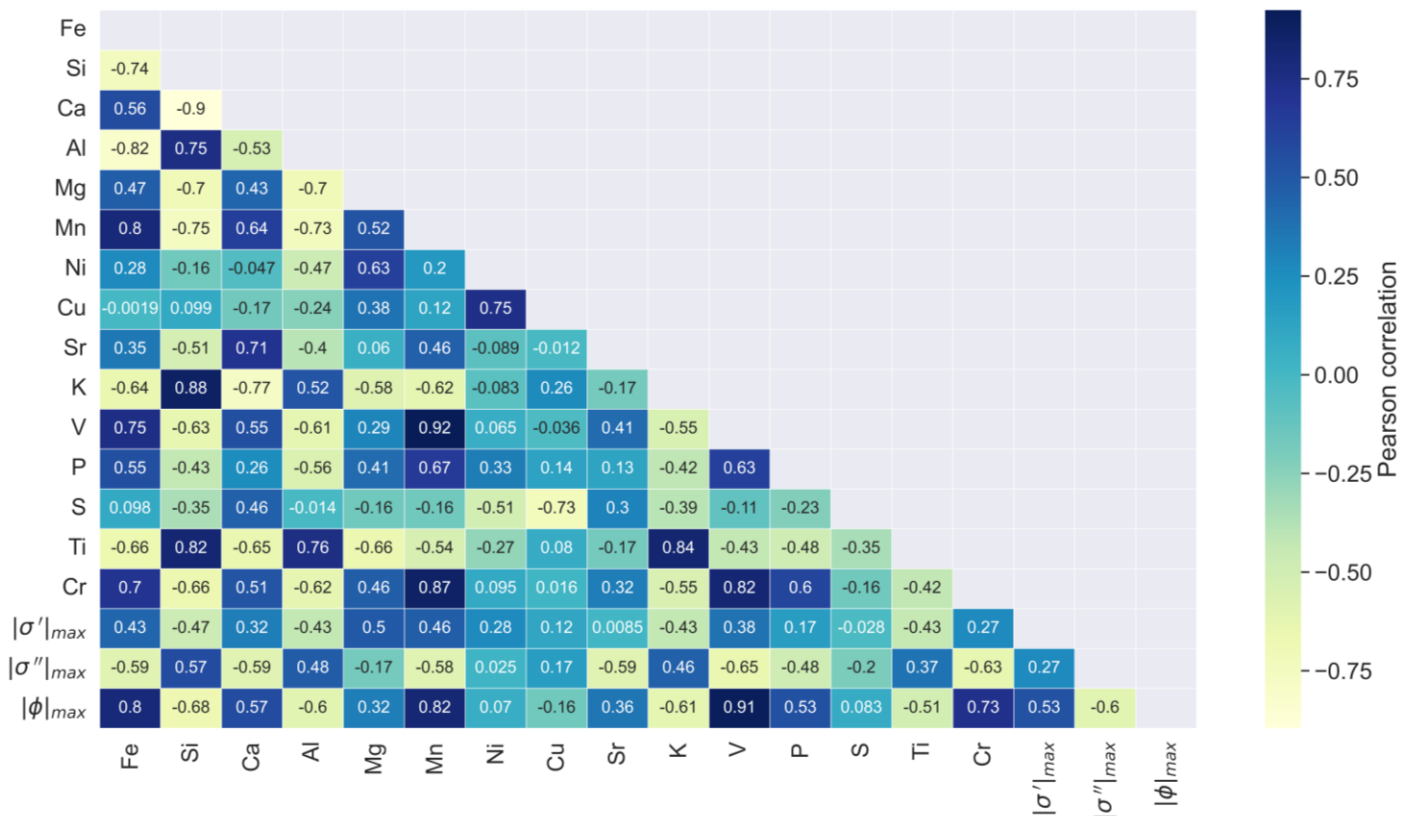


Figure 13: Pearson's correlation coefficient matrix of the average content of some elements and the geophysical data measured in all samples (magnitude of $\{\sigma', \sigma'', \Phi\}$ at the relaxation frequency or where the peak is observed).

In the correlation coefficient matrix of Figure 13 we can note that $|\sigma'|_{max}$ and $|\sigma''|_{max}$ do not present strong correlations with the average content of the elements nor between both geophysical variables. On the other hand, the strongest positive and negative correlations can be observed for the $|\Phi|_{max}$. The magnitude of the peak phase has strong positive correlations with the V, Mn, Fe and Cr while and it has intermediate negative correlations with the Si, Al, K and also with $|\sigma''|_{max}$. These results are similar to the previous section with the measurements in time-domain. Note that for most applications we can approximate the phase Φ with the ratio

between the imaginary and real components of the conductivity (Flores-Orozco et al. 2020), therefore the phase includes information about the energy loss (σ') and the energy storage (σ''). This is the reason why most of the negative and positive correlations between ρ and C in time-domain with the different elements, can be also observed between Φ and the same chemical elements.

4.2 FROM GEOPHYSICAL FIELD MEASUREMENTS

For an exhaustive revision of the data acquired on the site of Duferco, as well as data processing, results and interpretation, see deliverable D. I3.2.1. Here we used the 3D inverted models of resistivity (ρ) and chargeability (C) obtained in the slag heap (see Figure 14). We studied the correlations between the inverted values of ρ and C at the position where the samples were collected and the XRF results.

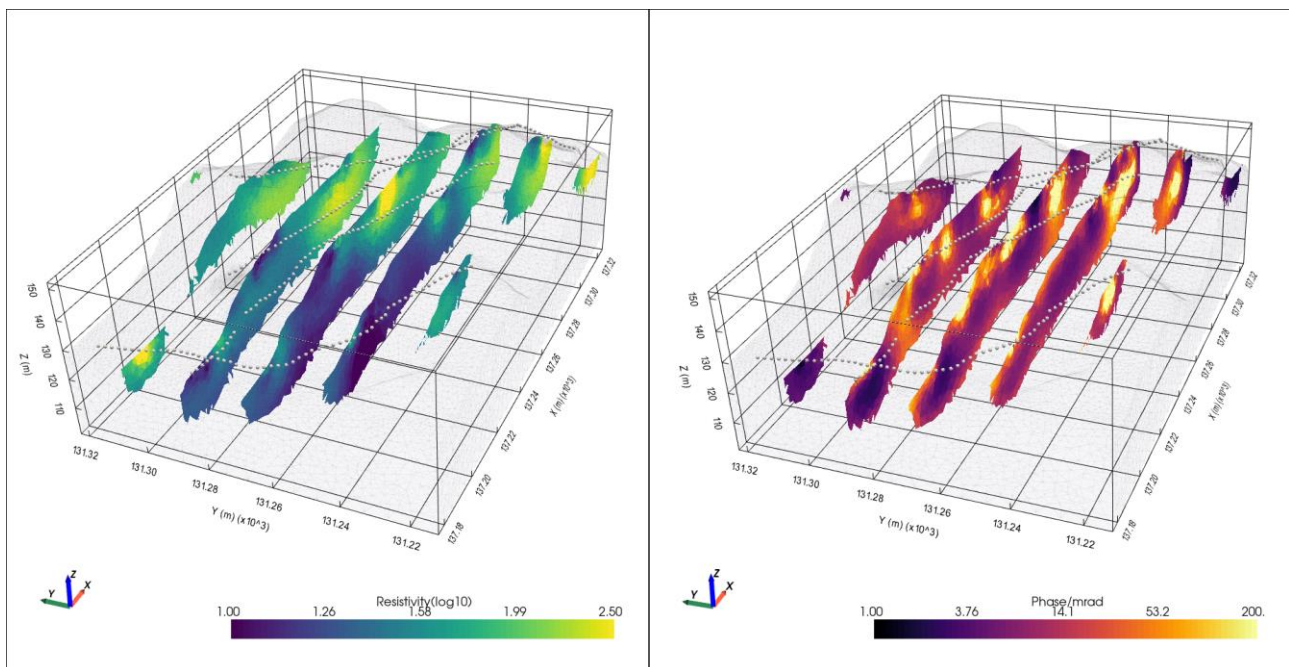


Figure 14: 3D inverted models of resistivity (left) and chargeability (right) obtained in the slag heap. We display several 2D sections across the Y-axis. The white spheres show the position of the electrodes.

Figure 15 shows the correlation matrix between the inverted values of ρ and C co-located with the samples and the average content of the different elements. The values of ρ and C considered here are the average of the values taken from the model within a volume defined by a prism of $1.5 * 1.5 * 0.8$ m centred at the point where the samples were collected. Additionally to observe spatial trends in the data we also include the positions at which all samples were taken $\{X, Y, Z\}$, e.g., to analyse if there is a correlation between the depths and the geophysical values or the concentration of certain element.

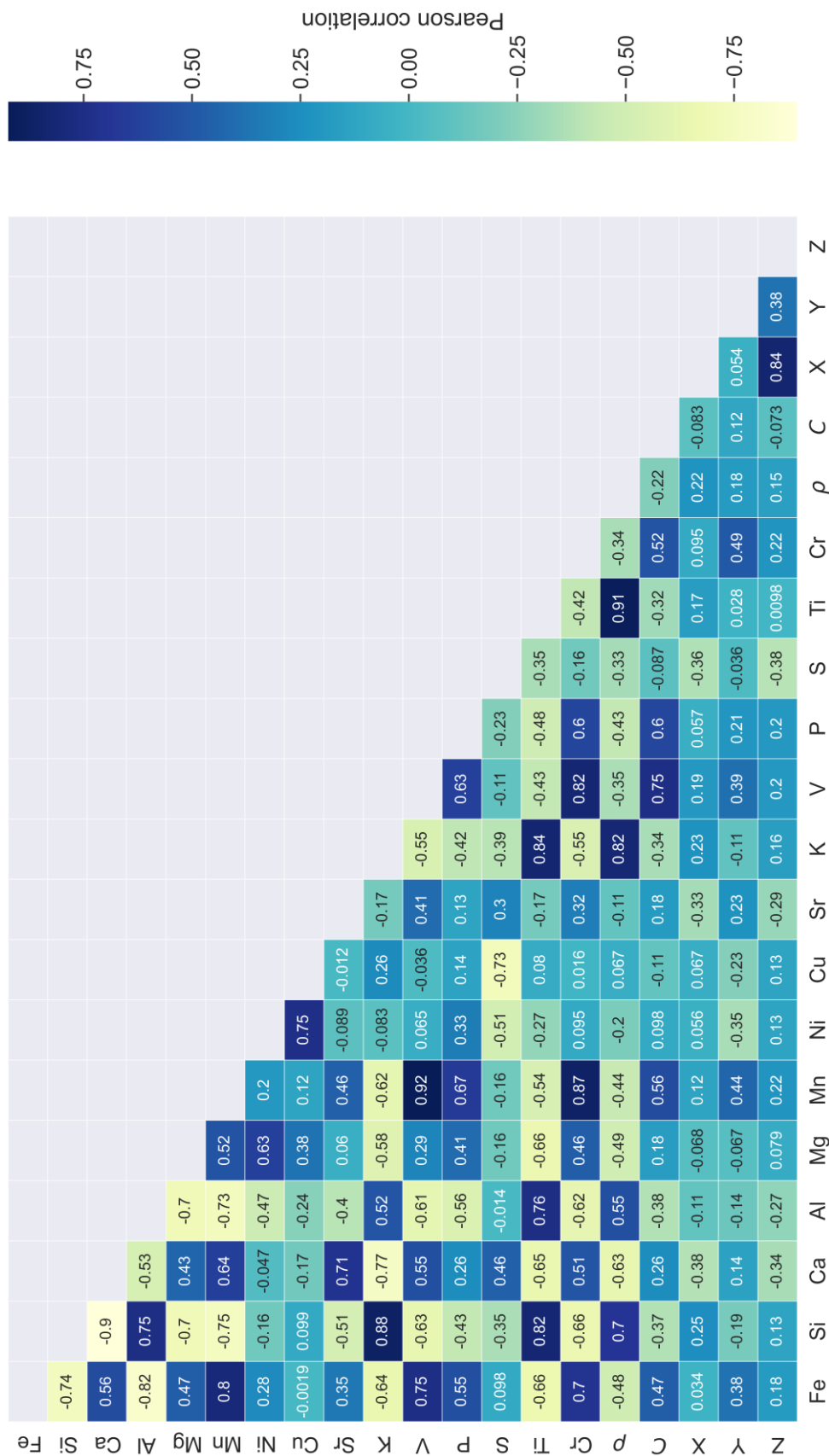


Figure 15: Pearson's correlation coefficient matrix of the average content of some elements and the geophysical inverted data co-located with the samples as well as the position {X, Y, Z} at which samples were taken.

For this last correlation matrix with the geophysical field data and spatial data we can make several observations. First, the resistivity values present strong positive correlations with the Si, K and Ti, which are the same correlations found with the lab measurements of ρ . In addition we can note that the correlation of V and P content are strong and positive with the chargeability from laboratory and field. However, the strength of the correlation decrease for the field geophysical data. Finally, the correlations between the positions of the samples $\{X, Y, Z\}$ and the chemical elements as well as the ones with the inverted geophysical values are very low. This means that there are no dominant elements with larger concentrations in specific locations or depths of the slag heap (at least up to a depth of 5 m at which the samples were collected).

5 CONCLUSIONS

The integrated approach developed within NWE-REGENERATIS to characterize former metallurgical sites and deposits has proved useful for the third pilot site of Duferco. In this report we describe the correlations between the geophysical measurements and the chemical analysis carried out by CTP. This analysis has been conducted using both field and laboratory geophysical measurements in order to analyze scale effects.

We observed stronger linear correlations between the geochemical analysis and the geophysical laboratory measurements than the correlations with field geophysical measurements. It is important to point out that laboratory measurements represent punctual values of ρ and C within a volume at a known depth while bulk ρ and C are measured using ERT and IP in the field - whose inverted model are inherently non-unique, i.e., measured data are explained equally well by an infinite number of subsurface models (Uhlemann et al. 2017). Despite a good consistency between laboratory and field geophysical data, these results show the small-scale geochemical variability of the Duferco deposits. Nevertheless, the strong correlations observed between the field measurements of ρ and some geochemical contents show the ability of the ERT/IP methods to image different types of materials.

This correlation analysis provides consistent dataset of geochemical content, laboratory and field geophysical measurements. This dataset constitutes an interesting outcome for the study of others past metallurgical site. The consistency of both field and laboratory geophysical data with geochemical analysis is an interesting result. In the future, first approximations could be done only with field geophysical data and geochemical analysis. Furthermore, this study demonstrates the importance of laboratory measurements to precisely estimate the relation between geochemical content and geophysical properties. This relation could be quite strong in function of some elements (Fe, Mn, V) but the small-scale variability of the deposit decreases this relation in the field.

Finally, this report presents strong evidence of geophysical properties linked with geochemical elements, which is one of the objectives of the NWE-REGENERATIS project. The correlations presented here represent a suitable basis to build the raw materials and pollution distribution model (RAPIDM), to delineate areas of interest and estimate volume(s).

6 REFERENCES

- Flores-Orozco, A., J. Gallistl, M. Steiner, C. Brandstätter, and J. Fellner. 2020. "Mapping Biogeochemically Active Zones in Landfills with Induced Polarization Imaging: The Heferlbach Landfill." *Waste Management* 107 (April): 121–32. <https://doi.org/10.1016/j.wasman.2020.04.001>.
- Florsch, Nicolas, M. Llubes, F. Téreygeol, A. Ghorbani, and P. Roblet. 2011. "Quantification of Slag Heap Volumes and Masses through the Use of Induced Polarization: Application to the Castel-Minier Site." *Journal of Archaeological Science* 38 (2): 438–51. <https://doi.org/10.1016/j.jas.2010.09.027>.
- Martin, Tina, Thomas Günther, Andreas Weller, and Kerstin Kuhn. 2021. "Classification of Slag Material by Spectral Induced Polarization Laboratory and Field Measurements." *Journal of Applied Geophysics* 194 (November): 104439. <https://doi.org/10.1016/j.jappgeo.2021.104439>.
- Placencia-Gómez, Edmundo, Annika Parviainen, Lee Slater, and Jussi Leveinen. 2015. "Spectral Induced Polarization (SIP) Response of Mine Tailings." *Journal of Contaminant Hydrology* 173 (February): 8–24. <https://doi.org/10.1016/j.jconhyd.2014.12.002>.
- Qi, Youzheng, Abdellahi Soueid Ahmed, André Revil, Ahmad Ghorbani, Feras Abdulsamad, Nicolas Florsch, and Jeremy Bonnenfant. 2018. "Induced Polarization Response of Porous Media with Metallic Particles — Part 7: Detection and Quantification of Buried Slag Heaps." *GEOPHYSICS* 83 (5): E277–91. <https://doi.org/10.1190/geo2017-0760.1>.
- Uhlemann, Sebastian, Oliver Kuras, Laura A. Richards, Emma Naden, and David A. Polya. 2017. "Electrical Resistivity Tomography Determines the Spatial Distribution of Clay Layer Thickness and Aquifer Vulnerability, Kandal Province, Cambodia." *Journal of Asian Earth Sciences* 147 (October): 402–14. <https://doi.org/10.1016/j.jseaes.2017.07.043>.
- Zimmermann, E., J. A. Huisman, A. Kemna, J. Berwix, W. Glaas, H. Meier, B. Wolters, and O. Esser. 2010. "Advanced Electrical Impedance Tomography System with High Phase Accuracy." *In* , 583–91. https://mail-attachment.googleusercontent.com/attachment/u/0/?ui=2&ik=6c448d5b30&view=att&th=14d004309bb05ea7&attid=0.1&disp=safe&realattid=f_i91d40t60&zw&saduie=AG9B_P9xdLHxnTB-5AFICsrBXodf&sadet=1430229033145&sadat=ANGjdJ_l2UMyW0tTGhzVrjihVjzhZ7sRgA2ESI5iYgKJfuWejL3qxL4CbN2dK9E&sads=m6E-UiklaqsBoXVUM_oBzNQdWrk.